A Layer Stripping Approach for EM Reconstruction of Stratified Media

Salvatore Caorsi, *Member, IEEE*, and Mattia Stasolla, *Member, IEEE*

***Abstract*—This paper presents an electromagnetic (EM) technique for the reconstruction of the physical and geometrical properties (permittivity and thickness) of stratified media. The key points of the approach, belonging to the so-called layer stripping algorithms, are the introduction of an equalization step that takes into account propagation effects, and the design of a procedure devoted to multiple reflections' removal. Furthermore, the proposed main processing block is an energy-based method able to accurately estimate amplitudes and time of delays of backscattered echoes in the time domain. A numerical analysis of the algorithm's potentialities will show that it can be successfully employed under different working conditions and in the presence of noisy data.**

***Index Terms*—Layer stripping (LS), multilayered media, nondestructive testing.**

I. Introduction

RADIOGLACIOLOGY, through-the-wall imaging, geological surveys, and infrastructure monitoring are only a few of the practical applications where nondestructive testing based on EM measurements can be the most appropriate solution [1]–[3].

The general problem consists in evaluating the physical and geometrical properties—in terms of permittivity and thickness—of a multilayered dielectric by means of its scattering data.

Among the most commonly employed techniques (for a comprehensive review, see [4]), the layer stripping (LS) approach has been extensively used over the years [5]–[8]. LS is a nonlinear method based on causality, where the multilayered dielectric is recursively reconstructed by determining the properties of one layer at a time and progressively removing the already reconstructed layers from the stack [9]. With respect to other methods, which are, in general, more accurate, the great interest in LS can be explained considering that it can provide high computational efficiency [10]. In particular, the approaches belonging to LS exploit the Schur recursions [11], a fast algorithm well suited to high-speed data processing, becoming a feasible solution for processing large amount of data in real time [12].

Manuscript received October 18, 2012; revised June 20, 2013; accepted November 23, 2013. Date of publication December 19, 2013; date of current version May 1, 2014.

S. Caorsi is with the Dipartimento di Ingegneria Industriale e dell' Informazione, University of Pavia, 27100 Pavia, Italy.

M. Stasolla was with the Dipartimento di Ingegneria Industriale e dell' Informazione, University of Pavia, 27100 Pavia, Italy. He is now with the Institute for the Protection and Security of the Citizen, Joint Research Centre, European Commission, 21027 Ispra, Italy (e-mail: mattia.stasolla@unipv.it).

Color versions of one or more of the figures in this paper are available online at http://ieeexplore.ieee.org.

Digital Object Identifier 10.1109/TGRS.2013.2293533

For this reason, the LS finds a straightforward employment in radar data inversion, where the analysis of EM signals can be carried out directly in the time domain. The generic processing scheme starts with the detection of the echoes reflected at each interface, and then, the amplitude and time of delay (TOD) of such echoes are evaluated and finally used to estimate the permittivity and thickness of the corresponding layers. In [13], LS has been successfully applied to permittivity measurements in multilayered media, in comparison with an inversion technique based on the minimization of the mean square error between measured and modeled data. In [14]–[16], it has been shown that LS is particularly suited for the ground penetrating radar (GPR) tracking of road pavements, typically composed of a fixed number of layers with standard dielectric and geometric characteristics. An LS approach has been also applied to the reconstruction of the vertical structure of an ice shelf, which could be modeled as a shallow layer of snow on top, glacial ice, a layer of salt ice, and the seawater [17].

Although characterized by different processing techniques, LS algorithms are typically based on a set of common assumptions that can be summarized as follows.

1) Propagating signals are assumed to be plane waves.
2) The presence of multiple reflections is neglected.

In addition, echo detection is mostly based on peak seeking or matched filtering techniques, which suffer a poor temporal resolution and therefore might not be able to manage overlapping echoes [18].

A few recent works have actually tried to explicitly face some of these open issues, but only focusing on the solution of a specific problem. In [19], a new GPR calibration method is proposed that aims at improving the measurement accuracy for the layer thickness and permittivity of multilayered pavements; in [20], clutter reduction techniques are applied to EM data acquired within a through-the-wall imaging application in order to suppress undesired reflections; in [21], the authors compare different superresolution methods able to improve the time resolution of GPR data.

To the best of our knowledge, no LS methodologies can be found in the literature that address the development of a general framework where propagation conditions, multiple reflections, and spatial resolution enhancement are handled.

The aim of this paper is therefore to provide a comprehensive solving approach by supplying the LS technique with additional features that can allow to overcome the aforementioned simplifications, and then evaluate to which extent this can yield improvements.

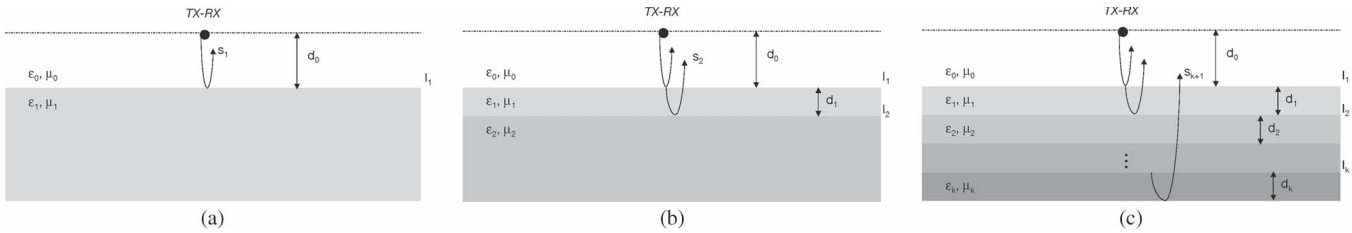

Fig. 1. Geometric modeling of the scenario: stratified medium is composed of k uniform lossless nondispersive layers.

In particular, the key points of this work are as follows:

1) introduction of an equalization step that takes into account propagation effects and compensates for losses in signal amplitudes;
2) implementation of a procedure to detect and classify multiple reflections in order to remove their effects on the received signals;
3) design of an energy-based method to accurately estimate amplitudes and TODs of backscattered echoes.

This paper is organized as follows. Section II is devoted to the formalization of the problem and the detailed description of the proposed LS algorithm. Section III discusses the influence of multiple reflections on the inversion process and provides a processing chain for the detection and classification of multiples which can be exploited to mitigate their effects. In Section IV, a numerical assessment of the method's potentialities is provided that shows how it can perform in different working conditions and in the presence of noisy data. Section V concludes this paper with comments and final remarks.

II. Methodology

A. Problem Formalization

Let us consider the scenario shown in Fig. 1(a), where a transmitting/receiving system is placed over an indefinite background L_1 of permittivity ε_1 at distance d_0. By feeding the transmitting antenna (TX) with a current/voltage pulse $m(t)$ and assuming a lossless and nondispersive background, we expect that the signal s_1 sensed at the receiver (RX) would have the form

$$s_1 = \mathcal{P}_1 \mathcal{R}_1 u(t - \tau_1) \tag{1}$$

where the term

— $\mathcal{P}_1$ models the free-space path loss, which is the signal attenuation related to wave propagation;
— $\mathcal{R}_1$ takes into account the effect of the air/background interface (I_1), namely, it is bound to the amplitude ratio between the incident wave and the reflected wave generated at that discontinuity;
— τ_1 represents the arrival time of the signal, whose delay depends on the distance covered by the wave with respect to its velocity;
— $u(t)$ is the received waveform, whose amplitude and shape are, in general, different from those of the excitation signal because of the impulse response of the TX–RX channel.

As can be noticed, $\mathcal{P}_1$, $\mathcal{R}_1$, and τ_1 are generic scenario-dependent functions (they will be referred to as "descriptors"), which are also related to the operational conditions of the illumination system.

From this viewpoint, the monostatic scheme assumes a particular interest due to its geometrical configuration, which allows to considerably simplify the modeling of wave propagation.

In fact, given that the distance d_0 is suitably chosen in order to place the background within the far-field region of the transmitting antenna, where the amplitude of the transmitted signal is inversely proportional to the distance from the source, we can easily write $\mathcal{P}_1 = \mathcal{P}_1(d_0) = 1/2d_0$. Moreover, in the far-field region, we can study the backscattering of the background interface by employing the well-known theory of plane wave reflection at normal incidence [22] and derive the reflection coefficient at interface I_1 so that $\mathcal{R}_1 = \mathcal{R}_1(\varepsilon_0, \varepsilon_1) = \varrho_1 = (\sqrt{\varepsilon_0} - \sqrt{\varepsilon_1})/(\sqrt{\varepsilon_0} + \sqrt{\varepsilon_1})$.

Finally, the arrival time of the received signal can be evaluated by considering that the EM wave is covering the TX–RX distance with a velocity that depends on the propagation medium. For signal s_1, we obtain $\tau_1 = \tau_1(d_0, \varepsilon_0) = 2d_0(\sqrt{\varepsilon_0}/c)$.

If we now give the layer L_1 a finite thickness d_1 and place a new lossless nondispersive indefinite background L_2 of permittivity ε_2 [see Fig. 1(b)], we will collect at the receiver, along with the signal s_1, a second echo s_2, which can be written as

$$s_2 = \mathcal{P}_2(d_0, d_1)\mathcal{T}_2\mathcal{R}_2(\varepsilon_1, \varepsilon_2)u\Big[t - \tau_2(d_0, d_1, \varepsilon_0, \varepsilon_1)\Big] \tag{2}$$

where the functions $\mathcal{P}_2$, $\mathcal{R}_2$, and τ_2 are analogous to $\mathcal{P}_1$, $\mathcal{R}_1$, and τ_1 but depend on d_0 and ε_0 and also on d_1 and ε_1. It can be seen that, differently from the previous case, the signal model in (2) involves a further term that quantifies the transmission at interface I_1 in both the downward and upward directions. Again, from theory, this contribution can be expressed as $\mathcal{T}_2 = \mathcal{T}_2(\varepsilon_0, \varepsilon_1) = 1 - \varrho_1^2$.

By iterating the procedure followed for s_1 and s_2, it is straightforward to generalize the above formulation to the total received waveform S_K generated by a stack of K layers [see Fig. 1(c)]

$$S_K = \sum_{k=1}^{K} s_k = \sum_{k=1}^{K} \mathcal{P}_k(\dot{d}_k)\mathcal{T}_k(\dot{\varepsilon_k})\mathcal{R}_k(\varepsilon_{k-1}, \varepsilon_k)u\Big[t - \tau_k(\dot{d}_k, \dot{\varepsilon_k})\Big] \tag{3}$$

where $\dot{d}_k$ and $\dot{\varepsilon}_k$ denote, for each layer k, the thickness and the permittivity of the 1st, 2nd, $\ldots$, $k-1$th layer, and[1]

$$\mathcal{P}_k = \frac{1}{2\sum_{i=0}^{k-1} d_i} \tag{4}$$

$$\mathcal{T}_k = \prod_{i=1}^{k-1} \left(1-\varrho_i^2\right); \qquad \mathcal{T}_1 = 1 \tag{5}$$

$$\text{with} \quad \varrho_i = \frac{\sqrt{\varepsilon_{i-1}} - \sqrt{\varepsilon_i}}{\sqrt{\varepsilon_{i-1}} + \sqrt{\varepsilon_i}} \quad \forall i > 0 \tag{6}$$

$$\mathcal{R}_k = \varrho_k \tag{7}$$

$$\tau_k = \frac{2}{c}\sum_{i=0}^{k-1} d_i \sqrt{\varepsilon_i}. \tag{8}$$

Equation (3) shows two interesting properties of the total received signal: 1) it can be seen as the sum of scaled and time-shifted replicas of a *base* waveform $u(t)$, and 2) the descriptors of each component s_k, except for $\mathcal{R}_k$, which depends on the dielectric constant of the layer reflecting the incident wave, are only functions of the upper layers' permittivities and thicknesses.

This suggests that the multilayered medium could be iteratively reconstructed in K steps by determining—starting from the first layer's reflection s_1—the descriptors for each signal s_k and inverting (6)–(8) to derive ε_k and d_{k-1}, respectively. Nevertheless, although the echoes s_k that form the received signal have time delays corresponding, by definition, to the descriptor τ_k, it is, in general, not possible to directly associate $\mathcal{P}_k$, $\mathcal{T}_k$, and $\mathcal{R}_k$ to their amplitudes.

We have already introduced, in fact, that the received waveform $u(t)$ is, in general, unknown, as it depends on how the excitation pulse is modified by the TX–RX channel impulse response, whose characterization is a critical issue due to many undesired effects that should be taken into account, e.g., variations of impedance between the antenna feed point, antenna, and air or ringing and coupling [4].

To avoid this problem, a preliminary phase is needed during which a reference signal $\hat{s}$ must be acquired. In fact, if a reference layer of known dielectric permittivity $\hat{\varepsilon}$ is illuminated from a distance $\hat{d}$, according to the previous discussion, the received signal would be

$$\hat{s} = \hat{\mathcal{P}}(\hat{d})\hat{\mathcal{R}}(\varepsilon_0, \hat{\varepsilon}) u\left[t - \hat{\tau}(\hat{d}, \varepsilon_0)\right]. \tag{9}$$

As $\hat{d}$, ε_0, and $\hat{\varepsilon}$ are given, the terms $\hat{\mathcal{P}}$, $\hat{\mathcal{R}}$, and $\hat{\tau}$ in (9) could be all determined (they have the same form as that of $\mathcal{P}_1$, $\mathcal{R}_1$, and τ_1) so that $u(t)$ could be directly evaluated. In this way, it would be therefore possible to measure the amplitude of each echo s_k and derive the descriptors for the corresponding layer. Once all the $\mathcal{P}_k$, $\mathcal{R}_k$, and τ_k have been determined, the properties of the multilayered medium are fully characterized by (4)–(9), and the problem is therefore reduced to the operational inversion of such equations, which will be discussed hereafter.

[1]In order to properly describe the actual propagation conditions, the radiated waves could be modeled as plane (p), cylindrical (c), or spherical (s)

$$\mathcal{P}_k^{(p)} = 1; \quad \mathcal{P}_k^{(c)} = \frac{1}{2\sum_{i=0}^{k-1}\sqrt{d_i}}; \quad \mathcal{P}_k^{(s)} = \frac{1}{2\sum_{i=0}^{k-1} d_i}.$$

B. Algorithm Description

For the inversion of the problem formulated in the previous part of this section, we here propose an energy-based solution that allows to disregard the direct evaluation of the *base* waveform $u(t)$ and—this will be discussed during the presentation of results—also provides a robust processing of the received signals.

In fact, for each component s_k of the total received signal, by defining Γ_k as the ratio $\mathcal{E}_k/\hat{\mathcal{E}}$ between the energy of the kth echo and the energy of the reference signal $\hat{s}$, we have that

$$\begin{aligned}\Gamma_k(t) &= \frac{\int_{\tau_k}^{\tau_k+t} s_k^2 dt}{\int_{\hat{\tau}}^{\hat{\tau}+t} \hat{s}^2 dt} = \frac{\int_{\tau_k}^{\tau_k+t} \mathcal{P}_k^2\mathcal{T}_k^2\mathcal{R}_k^2 u^2(t-\tau_k)dt}{\int_{\hat{\tau}}^{\hat{\tau}+t} \hat{\mathcal{P}}^2\hat{\mathcal{R}}^2 u^2(t-\hat{\tau})dt} \\ &= \frac{\mathcal{P}_k^2\mathcal{T}_k^2\mathcal{R}_k^2 \int_{\tau_k}^{\tau_k+t} u^2(t-\tau_k)dt}{\hat{\mathcal{P}}^2\hat{\mathcal{R}}^2 \int_{\hat{\tau}}^{\hat{\tau}+t} u^2(t-\hat{\tau})dt} \\ &= \xi_k \frac{\mathcal{R}_k^2(\varepsilon_{k-1}, \varepsilon_k)}{\hat{\mathcal{R}}^2(\varepsilon_0, \hat{\varepsilon})} \qquad \forall t < \Delta_k \end{aligned} \tag{10}$$

where $\Delta_k = \tau_{k+1} - \tau_k$ is the time interval between two subsequent echoes and $\xi_k = \mathcal{P}_k^2\mathcal{T}_k^2/\hat{\mathcal{P}}^2$ is an *equalization* term that takes into account the effects of propagation and transmission at interfaces.

The last term in (10) points out, as said, that the parameter Γ_k is totally independent of the $u(t)$ waveform. In addition, it provides the direct expression that allows to compute the reflection coefficient of the layer under test $\mathcal{R}_k$ (and therefore its permittivity ε_k) from $\hat{\mathcal{R}}$ and ξ_k, which are known quantities because they depend on the reference signal and on the already processed layers.

To get further into the processing details, the inversion algorithm can be itemized as follows.

1) First, the reference signal $\hat{s}$ is acquired, and its descriptors $\hat{\mathcal{P}}$, $\hat{\mathcal{R}}$, and $\hat{\tau}$ are determined.
2) Then, the received signal is scanned to detect τ_1, the arrival time of the first bounce, which can be easily determined by searching for the presence of nonzero values within the signal. Of course, it would be identical to $\hat{\tau}$ if the on-field analysis has the same setup as that of the preliminary phase.
3) Equation (8) must be used to determine d_0. This step is clearly not necessary for the first layer, but it is a part of the iterative procedure.
4) The values of d_0 and ε_0 shall be substituted in (4)–(5) in order to evaluate $\mathcal{P}_1$ and $\mathcal{T}_1$.
5) Starting from $\hat{\tau}$ and τ_1, the energies $\hat{\mathcal{E}}$ and $\mathcal{E}_1$ must be computed and then compared. Until no variations in the energy shape (with respect to the reference one) are revealed, no subsequent echoes have been received. On the contrary, when the energy values begin increasing, we are then able to detect τ_2, i.e., the arrival time of the second received echo.

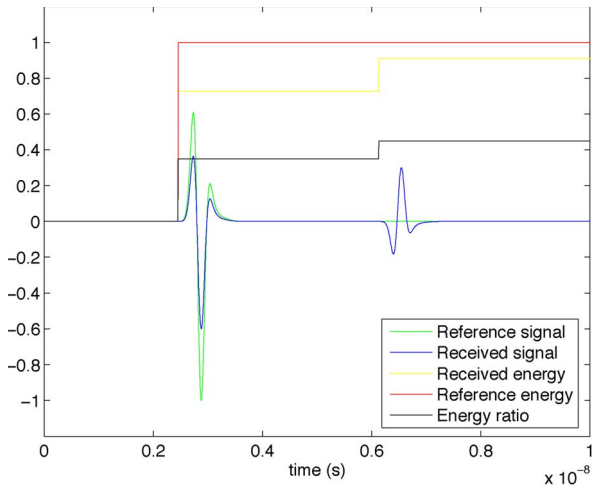

Fig. 2. Reference signal $\hat{s}$ and echoes s_1 and s_2. The corresponding energies and their ratio have been superimposed (all amplitudes have been normalized).

6) At this point, the computation of Γ_1 becomes straightforward, as it is simply the energy ratio $\mathcal{E}_1/\hat{\mathcal{E}}$ within the interval $[\tau_1, \tau_2[$ (see Fig. 2).
7) To obtain the desired value of ε_1, (10) should be inverted. To this end, we can combine $\hat{\mathcal{P}}$ and $\mathcal{P}_1$ with $\mathcal{T}_1$ to derive ξ_1. It must be noted that (10) gives the square value of $\mathcal{R}_k$, i.e., it does not provide any information about its sign. To overcome this drawback, it is sufficient to evaluate whether the current echo and the reference one are concordant so that $\mathrm{sgn}(s_k) = \mathrm{sgn}(s_k(t_s)) \oplus \mathrm{sgn}(\hat{s}(t_s))$, where t_s represents any instant within the time duration of the pulse and the symbol $\oplus$ denotes the XOR operator.
8) The signal values are set to 0 $\forall t < \tau_2$, and the procedure is repeated from step 3 until the last layer under test has been processed (at each iteration, the above subscripts "1" and "0" must be replaced with the current indexes k and $k-1$).

III. Multiple Reflections

In the previous section, we have shown that the reconstruction of the K permittivities and thicknesses of a stratified medium can be addressed by iteratively studying K independent subscenarios consisting of single layers placed above an indefinite background and illuminated by an EM wave.

Although such formulation allows to correctly evaluate the signals $s_1, s_2, \ldots, s_K$ representing the reflected waves generated at interfaces $I_1, I_2, \ldots, I_K$ by the incident wave during its transmission along the downward direction, it does not provide a complete description of the actual physical phenomenon.

In fact, if we rigorously consider each reflected and transmitted wave originating at discontinuities (irrespective of incidence direction) as a new source that illuminates the layers, we then have to model the infinite chain of signals that it produces. In particular, having assumed all lossless and nondispersive materials, these signals can do the following: 1) remain trapped within internal strata; 2) propagate indefinitely through the background; and 3) surface.

In the latter case, the receiver would acquire a train of undesired replicas of the *base* signal $u(t)$, which could potentially distort the total received signal and hinder the evaluation of S_K.

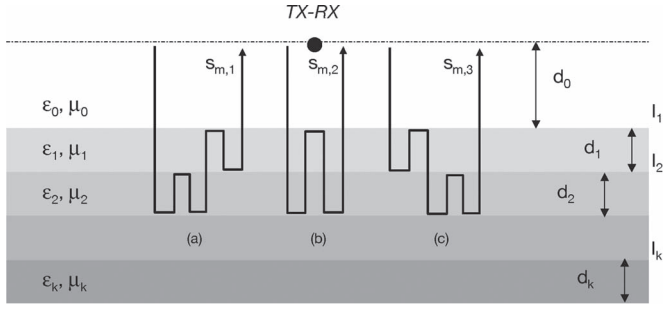

Fig. 3. Multiple reflections featuring the same arrival time and different propagation paths.

Keeping the notation used in the previous section, the train of *multiple reflections* that reaches the RX can be written as

$$S_M = \sum_m \sum_n s_{m,n} = \sum_m \sum_n \mathcal{P}_{m,n}\mathcal{T}_{m,n}\mathcal{R}_{m,n}u(t-\tau_m) \quad (11)$$

where m, n are positive integers and $\mathcal{P}_{m,n}$, $\mathcal{T}_{m,n}$, $\mathcal{R}_{m,n}$, and τ_m—which have the same form as that of $\mathcal{P}_k$, $\mathcal{T}_k$, $\mathcal{R}_k$, and τ_k—cannot be explicitly defined because of the infinite possible paths that the multiply reflected waves could take.

Differently from (3), where signals s_k are uniquely defined, the double summation over m, n in (11) is mandatory since it cannot be *a priori* excluded that the same electrical distance could be traveled along different paths. In fact, the subscript m is—as above—the progressive number of the echo within the pulse train, while the subscript n is necessary to identify echoes that may have arrived simultaneously.

To more easily understand the proposed notation, a graphical example is provided in Fig. 3, where three different signals $s_{m,1}$, $s_{m,2}$, and $s_{m,3}$ are assumed to reach the RX at a certain instant τ_m. As can be seen, the electrical distance covered is the same for all the paths (the wave travels twice in air and four times in both medium1 and medium2).

As said before, the presence of multiple reflections can hamper the reconstruction process proposed in the previous section, which is based on the signal model in (3). In fact, the actual received signal acquired at the receiver would therefore be

$$S_{TOT} = S_K + S_M = \sum_k \mathcal{P}_k\mathcal{T}_k\mathcal{R}_k u(t-\tau_k) + \sum_m \sum_n \mathcal{P}_{m,n}\mathcal{T}_{m,n}\mathcal{R}_{m,n}u(t-\tau_m). \quad (12)$$

To study how S_K and S_M can combine, it is useful to fix a certain τ_k and let τ_m vary within the interval $[\tau_k, \tau_{k+1}[$.

In this way, at each processing step k, only two possibilities may occur.

1) $\tau_m = \tau_k$

   At the receiver, we would not distinguish between the signal s_k and the signals $s_{k,n}$ because we would collect an equivalent signal $s_k^* = (\mathcal{P}_k\mathcal{T}_k\mathcal{R}_k + \sum_n \mathcal{P}_{k,n}\mathcal{T}_{k,n}\mathcal{R}_{k,n}) \cdot u(t-\tau_k)$. This would lead to a wrong evaluation of the relative permittivity of the kth layer.

2) $\tau_k < \tau_m < \tau_{k+1}$

In this case, the reconstruction of the kth layer would not be affected by errors, yet at time τ_m, the energy analysis would reveal a step within the profile. This means that, without a proper identification procedure, the multiple echo(s) $s_{m,n}$ would be misclassified as reflection from the $k+1$ layer.

According to these issues, the processing chain proposed in Section II becomes ineffectual in the presence of multiple reflections. Additional steps must be therefore supplied in order to manipulate the actual received signal and convert it to a signal analogous to S_K, i.e., composed uniquely of the direct reflections from interfaces.

The solution can be addressed by noting that, if multiple reflections occur before the signal s_k, they can only be due to the $k-1$ upper interfaces and that the τ_m is therefore a linear combination of the Δ_{k-1} intervals found during the analysis

$$\tau_m = \sum_{i=1}^{k-1} \alpha_i \Delta_i \qquad \text{with } \alpha_i \in \mathbb{N}. \tag{13}$$

The evidence of such relation can be immediately found in Fig. 3, where it is possible to observe that the arrival time τ_m of the three depicted signals is given, at step $k=4$, by $\alpha_1 = 1$ and $\alpha_2 = \alpha_3 = 2$. Moreover, with the signals $s_1, s_2, \ldots, s_k$ being the boundary cases characterized by $\alpha_1 = 1$, $\alpha_2 = 1, \ldots, \alpha_{k-1} = 1$, a constraint on the coefficients α_i directly comes, i.e., in the presence of multiple reflections at least one of them must be ≥ 2.

On this basis, the algorithm can be modified by simply adding a conditional statement at the end of step 3, which calls a subprocedure specifically designed for multiple reflection removal (MRR).

More in detail, at the end of iteration k, when the presence of a new echo is revealed at a certain time τ_x, (13) must be solved to find if there exists any set of α_i that gives exactly τ_x.

Case 1) If no combinations of α_i can be found that provide τ_m, then the current signal s_x necessarily corresponds to the reflection s_{k+1} from interface I_{k+1}, and it is possible to proceed to point 4.

Case 2) If a set of α_i exists that satisfies (13), then multiple reflections have occurred. Nevertheless, the presence of the echo from interface I_{k+1} cannot be directly excluded since suitable values of ε_{k+1} and d_{k+1} can be always found that yield a pulse reaching the RX at τ_x.

In order to resolve this ambiguity, the processing chain is supplied with a procedure that evaluates all the possible links that connect TX and RX under the constraints given by the calculated coefficients. In fact, only by knowing the exact paths traveled by the waves could we be able to reconstruct the signals $s_{x,n}$ that might have arrived at time $\tau_m = \tau_x$.

To this end, the authors have recently proposed [23] the construction of a binary decision tree, where each node is associated to a vertical level of the scenario (the TX/RX position or an interface) and splits into two children that represent the new levels that can be reached if either the upward reflected wave or the downward transmitted wave is considered. In this way, by selecting the subset of graph links corresponding to the physical paths from TX to RX, the propagation of multiple reflections can be fully characterized, and the signals $s_{x,n}$ can be modeled.

Once the signals $s_{x,n}$ are estimated, they must be subtracted from the original signal s_x.

1) If the residual is zero (or below a proper threshold), then no interface echo exists at τ_x. The subroutine halts, and the procedure restarts from point 3, in order to find a new incoming signal.
2) Otherwise, the subprocedure ends, and the main routine can now process a signal where all the spurious components have been removed. Steps 4–8 are then executed, and the current iteration is concluded.

IV. Results

In this section, a numerical assessment of the method's potentialities will be provided.

The data set employed for the tests has been created by means of GPRMax [24], a simulation software based on the finite-difference time-domain (FDTD) numerical method, and consists of a set of signals which simulate the field generated by an EM source illuminating a multilayered medium.

The TX/RX system is placed at a distance $d_0 = 35$ cm above the scenario. More in detail, the transmitting antenna has been modeled as a current line source fed with a differentiated Gaussian pulse (see Fig. 4(a), dashed line) of unitary amplitude and duration of 0.8 ns

$$f(t) = (\omega_p t)\exp\left[-\frac{(\omega_p t)^2 - 1}{2}\right] \rightleftharpoons$$
$$\mathcal{F}(\omega) = \left(j\sqrt{2\pi}\frac{\omega}{\omega_p^2}\right)\exp\left[-\frac{(\omega/\omega_p)^2 - 1}{2}\right]. \tag{14}$$

According to the Fourier pairs in (14), the feeding signal has a -10-dB bandwidth of about 5 GHz around a central frequency $f_p = w_p/2\pi = 2$ GHz (see Fig. 4(b), dashed line): This choice permits an acceptable tradeoff between pulse length and signal spectrum, in order to provide a satisfactory combination of penetration depth, spatial resolution, and homogeneity of materials. In fact, the emitted EM wave (see Fig. 4(a), solid line) is characterized by a duration of 1 ns and—correspondingly—a bandwidth of about 4 GHz with a central frequency 2.45 GHz. As regards the characterization of the scenarios, it should be noticed that, for our purposes, it is sufficient to analyze multilayered media composed of two uniform nondispersive layers above an indefinite background: the processing of any other deeper layers follows the same rationale and is therefore straightforward. The relative permittivity of the layers and their thicknesses have been chosen within the intervals: $\{\varepsilon_1, \varepsilon_2\} \in [2; 20]$ and $\{d_1, d_2\} \in [2; 20]$ cm.

We recall that the processing chain also requires a preliminary step for the acquisition of a reference echo backscattered by a layer of known permittivity. For the sake of simplicity, we opted for a *perfect electric conductor* (pec), which has well-known and convenient dielectric characteristics. To this end, a single layer scenario has been simulated.

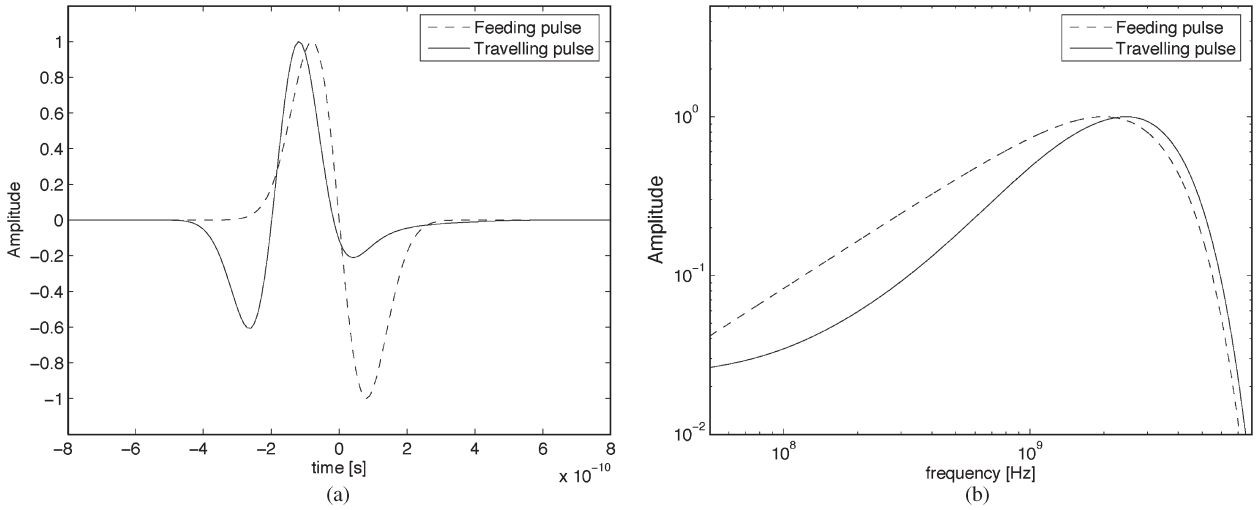

Fig. 4. (a) Feeding current pulse and traveling EM signal. (b) Corresponding Fourier transforms.

Finally, it is worth mentioning that, owing to the particular geometry, the numerical problem can be solved within the 2-D spatial domain, without appreciable losses in terms of accuracy but with a sensible reduction of computational costs [25].

A. Algorithm's Assessment

This first part of the assessment focuses on the evaluation of the reconstruction capabilities supplied by the method in the presence of separated interface echoes. For clarity, contributions from multiple reflections have been removed so that the signal sensed at the receiver is uniquely composed of interface reflections. In addition, as simulations have been carried out within a 2-D spatial domain, we will assume a cylindrical propagation model, where wave amplitudes decay proportionally to the square root of the distance [25].

As discussed in Section II-B, the inversion process for the kth echo is based on the evaluation of the reflection coefficient $\mathcal{R}_k$, which depends on the energy ratio Γ_k, the reflection coefficient $\hat{\mathcal{R}}$ of the reference layer, and the equalization parameter ξ_k.

In particular, with the reference layer being made of *pec*, by definition, we have that $\hat{\mathcal{R}} = -1$, and (10) reduces to

$$\Gamma_k = \xi_k \mathcal{R}_k^2. \tag{15}$$

To reconstruct the permittivity ε_k, we therefore only need to invert (15) by using Γ_k, directly computed from the received signal, and ξ_k, which is a function of the already reconstructed $k-1$ layers.

As far as the first layer is concerned, we have that

$$|\mathcal{R}_1| = |\varrho_1(\varepsilon_0, \varepsilon_1)| = \sqrt{\frac{\Gamma_1}{\xi_1}} = \sqrt{\frac{\Gamma_1(\varepsilon_0, \varepsilon_1)\hat{\mathcal{P}}^2(\hat{d})}{\mathcal{P}_1^2(d_0)}}. \tag{16}$$

Although not strictly required by the algorithm, we can choose the same acquisition setup in both preliminary and test phases ($\hat{d} = d_0$). In this way, $\hat{\mathcal{P}} = \mathcal{P}_1$, which means that the equalization parameter ξ_1 becomes equal to 1, losing any dependences on propagation conditions. The descriptor $\mathcal{R}_1$ is therefore simply equal to the square root of the parameter Γ_1.

TABLE I
PERFORMANCE ASSESSMENT: TWO LAYERS
(a) FIRST LAYER. (b) SECOND LAYER

	ε_1		Γ_1	
mean	0.13	1.06%	1.9e-3	0.42%
max	0.49	2.49%	3.7e-3	1.96%
min	6e-3	0.07%	0.1-3	0.03%
	$\mathbf{d_1}[mm]$		$\tau_2[\mathbf{ps}]$	
mean	0.5	0.43%	5.3	0.11%
max	1.5	0.84%	15.5	0.20%
min	0.0	0.00%	0.0	0.0%

(a)

	ε_2		Γ_2	
mean	0.51	3.93%	8.0e-3	4.69%
max	2.20	12.17%	27.5e-3	9.64%
min	0.01	0.23%	0.1e-3	0.11%
	$\mathbf{d_2}[mm]$		$\tau_3[\mathbf{ps}]$	
mean	1.1	1.38%	34.2	0.43%
max	4.2	9.19%	184.2	2.45%
min	0.0	0.00%	0.5	0.01%

(b)

The upper part of Table I(a) reports the absolute and relative errors[2] for the parameter Γ_1 with respect to the theoretical values given by the expected reflection coefficient ϱ_1. As can be seen, the medium percentage error is below 0.5%, and even the maximum error does not exceed 2%. In terms of permittivity reconstruction, this yields the excellent mean relative error of 1% and a maximum error of 2.5%; it is worth mentioning also the maximum absolute error, which is only 0.5.

As already explained, the same processing step for the computation of Γ_1 also provides the delay τ_2 of the new incoming echo. This delay must be employed to derive the thickness of the first layer, according to (8).

In the bottom part of Table I(a), it can be found that the detection of the second echo is performed very accurately—with a time shift of a few picoseconds—allowing a very precise reconstruction of the medium's thickness: along with a mean

[2]The percentage relative error of the output x with respect to the reference input $\hat{x}$ has been computed according to the following formula:

$$err(x) = \frac{|\hat{x} - x|}{|\hat{x}|} \times 100.$$

relative error of 0.4%, the maximum error remains below the outstanding value of 0.92%, which means that thickness can be provided with a tolerance of ± 1.5 mm.

When ε_1, d_1, and τ_1 have been determined, the second echo can be processed. As in the previous case, we can write

$$|\mathcal{R}_2| = |\varrho_2(\varepsilon_1, \varepsilon_2)| = \sqrt{\frac{\Gamma_2}{\xi_2}} = \sqrt{\frac{\Gamma_2(\varepsilon_0, \varepsilon_1)\hat{\mathcal{P}}^2(\hat{d})\mathcal{T}_1^2(\varepsilon_0, \varepsilon_1)}{\mathcal{P}_2^2(d_0, d_1)}}. \tag{17}$$

Since the equalization parameter is here $\neq 1$, we expect a worsening of the overall performances, biased by possible errors in the reconstruction of ε_1 and d_1 at the previous iteration.

The quantitative assessment of such effect is proposed in Table I(b), which shows a slight increase of the mean relative error from 1% to 4%. The maximum percentage error is more noticeable, which is 12%, whereas in absolute terms, the maximum mismatch is about 2.

Due to the specific processing technique, which restarts at each step the seeking procedure for incoming signals, the aforementioned drawback is less critical in thickness reconstruction. Table I(b) confirms a mean error increase in delay detection, from 0.4% to 1.4%, but this anyway guarantees a satisfactory tolerance in terms of thickness of a very few millimeters.

A further aspect that should be taken into account to explain the achieved results is that errors can be partly ascribed to an undesired nonphysical effect inherently present in the FDTD algorithm called "numerical dispersion" [26]. Briefly, it causes a shape distortion of the pulses propagating through the FDTD lattice due to the different phase velocities of the signal frequency components, a distortion that clearly hinders the reconstruction process. In case of cubical cells, the error introduced by numerical dispersion is inversely proportional to the points per wavelength [27], defined as $N_\lambda = \lambda/\Delta_x$; thus, in order to reduce such effect, the cell size should be chosen much smaller than the pulse wavelengths.

B. Propagation Model

We have just shown that a critical aspect of the inversion algorithm is the correct evaluation of the equalization parameter ξ_k. As expressed by (10), this parameter does not depend only on the vertical profile (permittivity and thickness) of the multilayered medium but also on the model chosen to describe wave propagation.

It is evident that the cylindrical model employed in the previous section could not be still valid for the processing of 3-D simulations or on-field data. Analogously, the commonly used simplification that employs plane wave propagation to reduce algorithms' complexity is not properly suited to describe the actual physical phenomenon. It would be therefore interesting to evaluate how the choice of a wrong propagation model can influence the overall performances. To this end, the processing of the entire data set has been replicated substituting the equalization parameter $\xi_k^{(c)} = \xi(\mathcal{P}_k^{(c)})$ with $\xi_k^{(p)} = \xi_k(\mathcal{P}_k^{(p)})$ and $\xi_k^{(s)} = \xi_k(\mathcal{P}_k^{(s)})$.[3]

[3]See note 1.

TABLE II
PERFORMANCE ASSESSMENT: PROPAGATION MODEL
(a) FIRST LAYER. (b) SECOND LAYER

	Spherical		**P**lane		**C**ylindrical	
	ε_1		ε_1		ε_1	
mean	0.13	1.06%	0.13	1.06%	0.13	1.06%
max	0.49	2.49%	0.49	2.49%	0.49	2.49%
min	6e-3	0.07%	6e-3	0.07%	6e-3	0.07%
	$\mathbf{d_1}[mm]$		$\mathbf{d_1}[mm]$		$\mathbf{d_1}[mm]$	
mean	0.5	0.43%	0.5	0.43%	0.5	0.43%
max	1.5	0.84%	1.5	0.84%	1.5	0.84%
min	0.0	0.00%	0.0	0.00%	0.0	0.00%

(a)

	Spherical		**P**lane		**C**ylindrical	
	ε_2		ε_2		ε_2	
mean	1.89	15.11%	0.68	6.66%	0.51	3.93%
max	9.93	64.31%	2.45	27.22%	2.20	12.17%
min	0.05	0.38%	0.00	0.00%	0.01	0.23%
	$\mathbf{d_2}[mm]$		$\mathbf{d_2}[mm]$		$\mathbf{d_2}[mm]$	
mean	4.0	4.15%	1.9	2.14%	1.1	1.38%
max	53.8	53.76%	18.2	15.19%	4.2	9.19%
min	0.1	0.17%	0.00	0.10%	0.0	0.00%

(b)

The numerical assessment, presented in Table II, shows that, as far as the first layer is concerned, reconstruction errors are both identical to those obtained for the cylindrical model. This should not surprise since the system has been intentionally arranged to provide an equalization parameter ξ_1 independent of propagation conditions. If we observe the errors returned after the processing of the second layer, instead, we can notice that both spherical and plane wave approximations (let us say "case S" and "case P," respectively) perform worse than the cylindrical model ("case C"). In particular, the mean permittivity error is almost twice in case P, and even four times in case S, whereas the layer's thickness increases to 2.14% in case P and to 4.15% in case S.

The reason for such behavior can be better explained by looking at graphs in Fig. 5. According to the thickness range chosen for our simulations, the distance covered by the EM signal is theoretically comprised between 0.78 and 1.50 m. As can be seen in Fig. 5(a), the random generation of scenarios has centered the values mostly within the interval $0.90 \div 1.1$ m, i.e., where the plane wave approximation is closer to the cylindrical one [see Fig. 5(b)]. This does not anyway mean that the plane model is, in general, better than the spherical one, but it confirms that the choice of an appropriate propagation model could improve the effectiveness of the method.

C. Overlapping Signals

Another important aspect that should be examined is the method's capability of resolving overlapping echoes.

For the sake of clarity, in the previous examples, we studied received signals featuring separate reflections; nevertheless, this condition holds true only if the delay between two subsequent echoes $\Delta_k = \tau_{k+1} - \tau_k \geq \Delta_p$, where Δ_p is the time duration of the traveling pulse.

The value of Δ_p is very important since it determines the spatial resolution that can be achieved. Therefore, depending on the scenario's characteristics, we must choose a signal wavelet consistent with the minimum dimensions that we need to resolve.

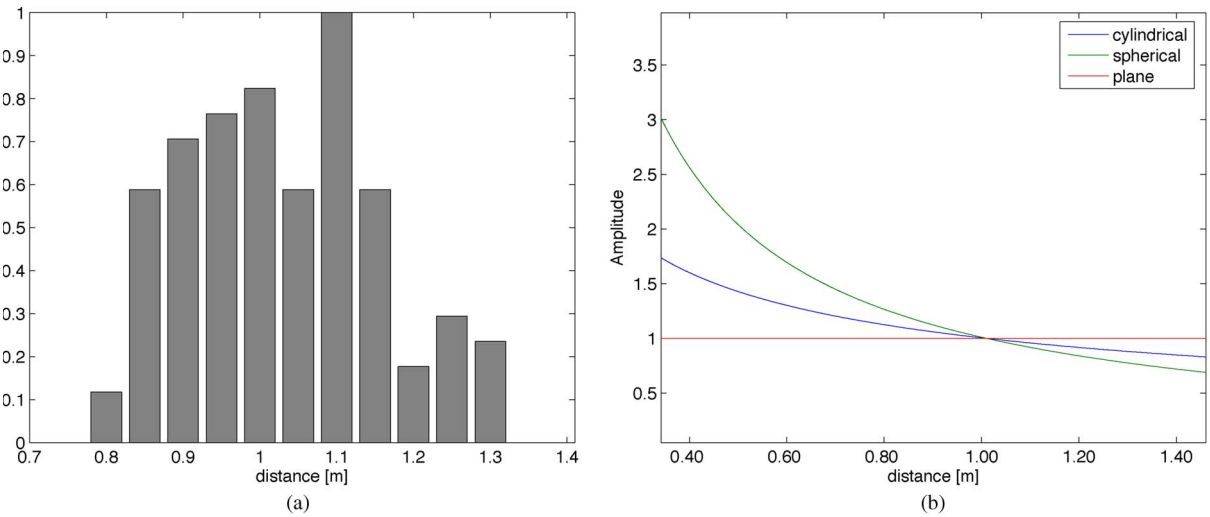

Fig. 5. (a) Distribution of layer's thickness for the simulated data set. (b) Cylindrical, plane, and spherical decays.

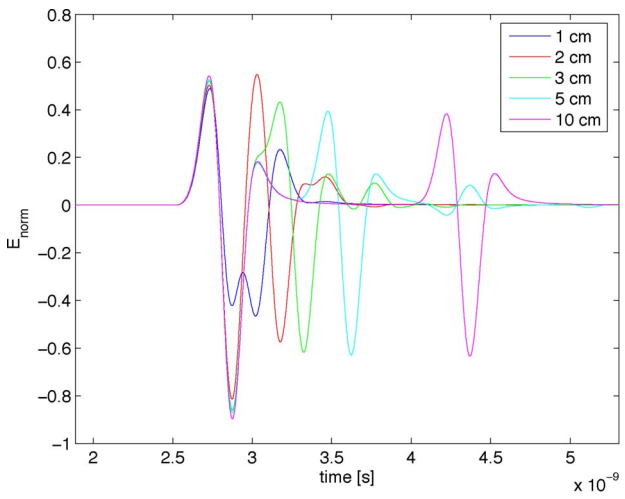

Fig. 6. Signals backscattered by layers with fixed permittivity and increasing thickness, illuminated by a 1-ns pulse.

This means that, for instance, if we are interested in detecting thin and/or transparent layers, we should employ a wideband signal, whereas in case of greater objects, a signal with a narrower band could be sufficient. If the choice of Δ_p is not correct, the received echoes may overlap, and the resulting waveform distortion would avoid a proper evaluation of amplitudes and time delays of the signals, affecting the reconstruction process. This can be immediately seen in Fig. 6, which depicts the signal backscattered by a single layer with $\varepsilon_1 = 5$ and increasing thickness $d_1 = 1, 2, 3, 5,$ and 10 cm, illuminated by a 1-ns pulse: The thinner the layer, the more unintelligible the echoes, which start overlapping when thickness is less than 5 cm.

To study the effects of the signal bandwidth on the overall performances, we tried to reconstruct the aforementioned scenario with three different signals obtained by setting the central frequency f_p in (14) as follows:

$$\text{SG1}: f_{p_1} = 2\ \text{GHz} \Longrightarrow \text{BW1} \sim 4\ \text{GHz}$$
$$\text{SG2}: f_{p_2} = 1\ \text{GHz} \Longrightarrow \text{BW2} \sim 2\ \text{GHz}$$
$$\text{SG3}: f_{p_3} = 500\ \text{MHz} \Longrightarrow \text{BW1} \sim 1\ \text{GHz}.$$

The wavelets and their corresponding spectra are shown in Fig. 7.

As far as the first signal is concerned, Table III(a) shows that the extraction technique seems not to suffer the waveform's distortion. In fact, it can be seen that, with thicknesses greater than 2 cm, the relative error in permittivity reconstruction is lower than 8%, and even in the very critical case of 1 cm, it is 13%, which means, in absolute terms, a difference of only 0.66. This is a noteworthy result if we consider the sensible interference between the first and the second echo (the resulting signal is outlined in "blue").

Such case is particularly interesting because it stresses the potentiality of the technique: typical approaches based on *peak seeking*, in fact, would associate the signal peak to the response of a material with lower permittivity, leading to a mistaken conclusion.

The algorithm keeps its effectiveness also when searching for arrival times and, therefore, in reconstructing layer thickness. Results are totally in line with previously discussed ones, also for the case of $x_L = 1$ cm. Even though the relative error increases to 8%, the absolute error can be quantified in only a few millimeters, so performances are very satisfactory.

If we look at the analogous results reported in Table III(b) and (c), we can find that, as expected, the 1-cm spatial resolution provided by SG1 cannot be achieved with SG2 and SG3. In particular, by employing SG2, it is possible to accurately reconstruct the permittivity of layers with thicknesses greater than 3 cm; the errors rise up to 17% for a layer of 2 cm, which is the minimum dimension that can be resolved. This threshold is clearly higher for SG3, whose length does not allow to detect layers thinner than 3 cm; it anyway remains a noticeable value. In both cases, the errors on thickness are very low within the entire resolution range.

D. MRR

This part of the numerical section deals with the issue of multiple reflections.

In Fig. 8, a simple received signal is presented, which has been generated by a multilayered scenario composed of two

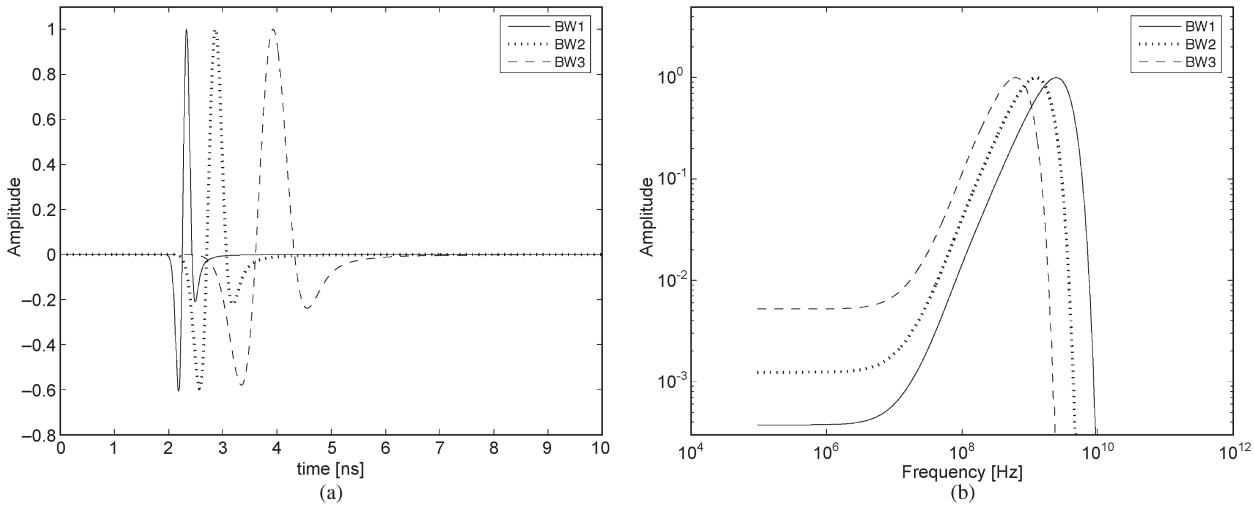

Fig. 7. (a) Signal wavelets for $f_p = 2.0, 1.0,$ and 0.5 GHz. (b) Corresponding spectra.

TABLE III
PERFORMANCE ASSESSMENT: OVERLAPPING SIGNALS (a) SG1. (b) SG2. (c) SG3

BW1 ∼ 4 GHz					
$\mathbf{d_1}$	$\mathrm{d_{1_{rec}}}$	$\delta_{\mathbf{d}_{\%}}$	$\varepsilon_{1_{rec}}$	ε_1	$\delta_{\varepsilon_{\%}}$
1 cm	0.92 cm	7.79%	5.00	5.66	13.2%
2 cm	1.93 cm	3.90%	5.00	5.38	7.59%
3 cm	2.96 cm	1.45%	5.00	5.17	3.41%
5 cm	4.97 cm	0.52%	5.00	5.02	0.40%
10 cm	9.98 cm	0.21%	5.00	5.02	0.40%
20 cm	19.99 cm	0.04%	5.00	5.02	0.40%

(a)

BW2 ∼ 2 GHz					
$\mathbf{d_1}$	$\mathrm{d_{1_{rec}}}$	$\delta_{\mathbf{d}_{\%}}$	$\varepsilon_{1_{rec}}$	ε_1	$\delta_{\varepsilon_{\%}}$
1 cm	-	-	-	-	-
2 cm	1.84 cm	7.99%	5.00	5.85	17.13%
3 cm	2.88 cm	3.84%	5.00	5.43	8.65%
5 cm	4.95 cm	0.94%	5.00	5.06	1.26%
10 cm	9.98 cm	0.21%	5.00	5.02	0.40%
20 cm	19.99 cm	0.04%	5.00	5.02	0.40%

(b)

BW3 ∼ 1 GHz					
$\mathbf{d_1}$	$\mathrm{d_{1_{rec}}}$	$\delta_{\mathbf{d}_{\%}}$	$\varepsilon_{1_{rec}}$	ε_1	$\delta_{\varepsilon_{\%}}$
1 cm	-	-	-	-	-
2 cm	-	-	-	-	-
3 cm	2.75 cm	8.48%	5.00	5.99	19.90%
5 cm	4.95 cm	0.94%	5.00	5.27	5.54%
10 cm	9.98 cm	0.21%	5.00	5.02	0.40%
20 cm	19.99 cm	0.04%	5.00	5.02	0.40%

(c)

layers with permittivities $\varepsilon_1 = 7$ and $\varepsilon_2 = 17$ and thicknesses $d_1 = 19$ cm and $d_2 = 17$ cm. This example can immediately show how the reconstruction process might be hindered by the presence of multiples. In fact, if we interpreted all the four backscattered echoes as direct reflections from layers' interfaces (the latter being the reflection from the background, which we are not interested in), we would then reconstruct a medium composed of three different slabs, as depicted in Fig. 9(a). As discussed in Section III, the total received signal can also contain multiples: by applying the MRR procedure, we would find that the third echo of Fig. 8 has not been directly backscattered by interface I_3 but multiply reflected by interfaces I_1 and I_2.

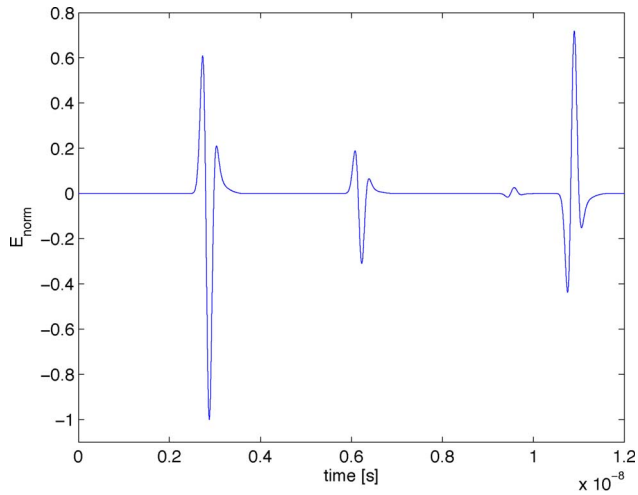

Fig. 8. Received signal composed of four echoes: without taking into account the presence of multiples, a wrong reconstruction could be carried out (see Fig. 9).

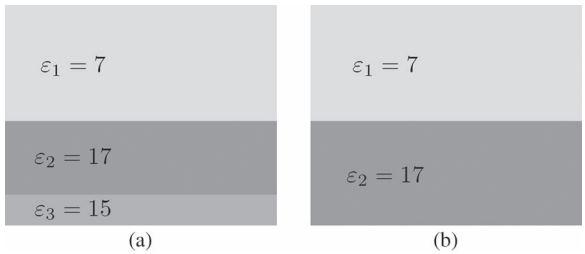

Fig. 9. Reconstruction of the received signal shown in Fig. 8: (a) Without MRR and (b) with MRR.

For this reason, a proper evaluation of the vertical profile of the medium needs to discard the multiple (for the proposed example, it is sufficient to window the signal) and consider the fourth echo as the direct reflection from interface I_3. The correct reconstruction of the scenario therefore results in a two-layer medium, shown in Fig. 9(b).

Another condition that can occur and limit the reconstruction process is when a direct reflection and a multiple feature the same arrival time. If we consider, for instance, a signal where

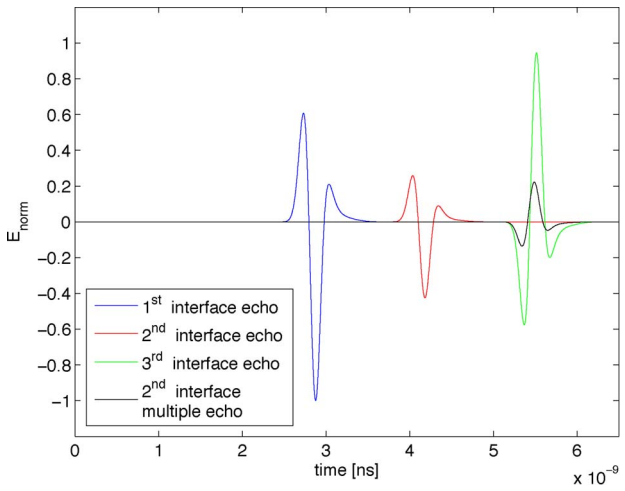

Fig. 10. Received signal where the direct reflection from a layer's interface and a multiple feature the same arrival time.

TABLE IV
PERFORMANCE ASSESSMENT: MRR (SINGLE CASE IN FIG. 10)

	Raw signal			M.R.R.		
	ε_{rec}	δ_ε	$\delta_{\varepsilon_\%}$	ε_{rec}	δ_ε	$\delta_{\varepsilon_\%}$
$\varepsilon_1 =$ **6**	5.96	0.03	0.56%	5.96	0.03	0.56%
$\varepsilon_2 =$ **16**	17.01	1.01	6.33%	17.01	1.01	6.33%
$\varepsilon_3 =$ **2**	1.59	0.41	20.07%	1.81	0.19	9.47%

TABLE V
PERFORMANCE ASSESSMENT: MRR (ENTIRE DATA SET)

ε_3	Raw signal		M.R.R.	
	δ_ε	$\delta_{\varepsilon_\%}$	δ_ε	$\delta_{\varepsilon_\%}$
mean	1.89	17.28%	0.89	8.17%
max	3.28	67.73%	1.55	16.74%
min	0.51	0.24%	0.24	0.21%

the third echo is the sum of the direct reflection from interface I_3 and a multiple (see Fig. 10), without identifying the presence of the multiple, we would then evaluate a wrong value of permittivity for the third layer.

Table IV points out that, by employing the MRR subroutine for the processing of the signal in Fig. 10, it is possible to strongly reduce the relative error for ε_3 from 20% to 9%. A detailed analysis carried out on the entire data set has provided (see Table V) that the improvements yielded by MRR to the reconstruction of those signals where the backscattering of the third layer is corrupted by multiples can be quantified in a reduction almost by half of the mean relative error from 17% to 8%, corresponding to an absolute error decreasing from 1.9 to 0.9. A noticeable effect is also induced to the maximum error, which drops off from 67% to 16%.

E. Noisy Data

In this paragraph, the processing chain is input with noisy data, in order to provide an assessment of the algorithm's response to experimental data.

The whole data set has been therefore corrupted with additive white Gaussian noise (AWGN) and then reprocessed as in Section IV-A to reconstruct permittivities and thicknesses of the scenario.

TABLE VI
PERFORMANCE ASSESSMENT: NOISY DATA

SNR		ε_1	$\mathbf{d_1}$	ε_2	$\mathbf{d_2}$
	mean	13.07%	4.62%	36.06%	9.95%
5 dB	max	43.66%	20.15%	178.51%	100.00%
	min	0.71%	0.06%	1.28%	0.11%
	mean	9.86%	3.08%	22.49%	7.33%
10 dB	max	47.78%	22.51%	159.45%	35.13%
	min	0.15%	0.05%	0.53%	0.035%
	mean	5.22%	2.12%	17.22%	3.64%
20 dB	max	21.83%	13.50%	295.58%	19.43%
	min	0.17%	0.00%	0.01%	0.16%
	mean	3.20%	1.46%	8.70%	2.78%
30 dB	max	10.84%	7.50%	104.73%	15.40%
	min	0.00%	0.10%	0.05%	0.10%
	mean	2.15%	0.93%	5.25%	1.81%
40 dB	max	10.97%	2.59%	52.02%	9.36%
	min	0.01%	0.00%	0.29%	0.00%

In particular, with

$$s_S(t) = \sum_s s_s = \sum_s A_s u(t - \tau_s) \tag{18}$$

being the simulated signal, we can model the new signal as

$$s_{SN}(t) = \sum_s A_s u(t - \tau_s) + \mathcal{N}\left(0, \sigma_n^2\right) \tag{19}$$

with $\mathcal{N}(\cdot)$ being the zero-mean Gaussian distribution with variance σ_n^2. Since the energy of each pulse is $P_s = E[s_s^2(t)] = \sigma_s^2$, we can write the corresponding signal-to-noise ratio (SNR) as $A_s^2\sigma_u^2/\sigma_n^2$.

For the assessment, we generated large sequences of noise samples according to five different levels of SNR (5, 10, 20, 30, and 40 dB), ultimately providing the averaged values of mean, maximum, and minimum errors obtained for each level.

Results, proposed in Table VI, show that the overall performances can be considered satisfactory even in the presence of corrupted data. As far as permittivity reconstruction is concerned, we can notice that, for almost all SNR levels, the mean error on ε_1 is below 10%, and even in the worst case of 5-dB SNR, which significantly distorts the signal's waveform (see Fig. 11), it does not exceed 15%. Nevertheless, the reconstruction of ε_2, as in the noiseless case, starts suffering error propagation from the upper layer, with error values which are 2–3 times higher and remain acceptable only for SNRs greater than 20 dB. For this reason, in the presence of very noisy signals, only a few layers could be effectively processed.

Differently, the method seems quite insensitive to such problem when reconstructing the layer's thickness. As already said, the procedure for the detection of echoes' arrival time is initialized at each iteration, and it is sufficiently robust to smooth the effect of undesired fluctuations within data. We can, in fact, observe that, for both layers, the average errors are very low (even at 5 dB, where the error is only 5% for d_1 and 10% for d_2, biased by the error on ε_2).

The overall trend of the method's performances versus SNR values has been sketched in Fig. 12, where the bar graph representing the mean error values illustrates that the higher the SNR, the higher the accuracy, with values at 40 dB comparable to those achieved in the presence of noiseless data.

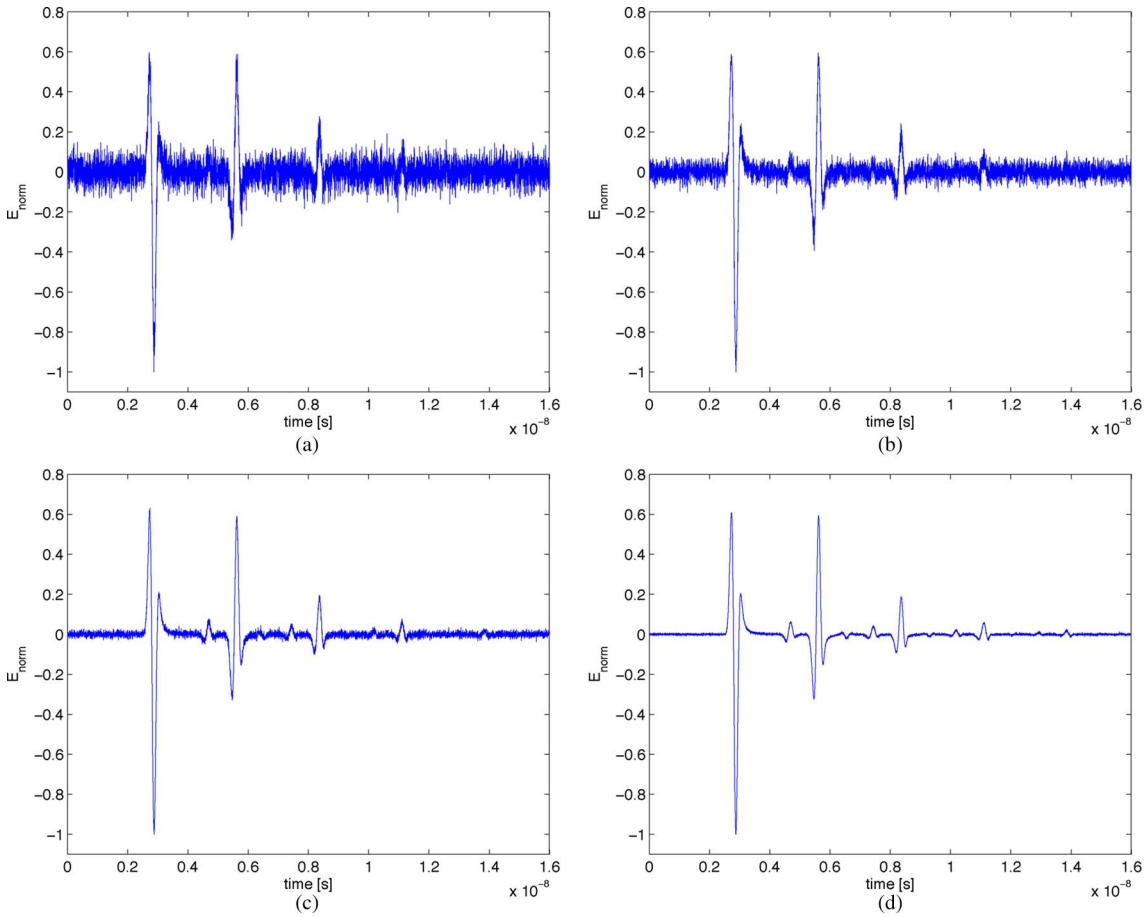

Fig. 11. Signals corrupted with additive white Gaussian noise (different levels of SNR are shown). (a) 5 dB. (b) 10 dB. (c) 20 dB. (d) 30 dB.

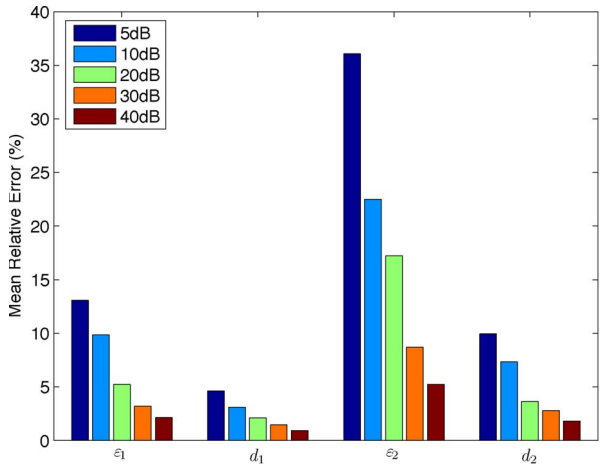

Fig. 12. Mean reconstruction errors versus SNR.

F. Conductivity

To further assess the performances of the method, we here propose a quantitative evaluation of how the presence of lossy media may influence the overall results.

We recall that the method is based on the assumption of lossless nondispersive media; thus, the inversion of signals generated by layers featuring nonzero conductivity will provide an intrinsic mismatch between actual and reconstructed values of permittivity and thickness.

In fact, the hypothesis of lossless media allows to consider the permittivity of the layers as a real quantity so that, for each layer k, we can determine ε_k and d_k by means of the following descriptors:

$$\mathcal{P}_k = \mathcal{P}_k(\dot{d}_k) \tag{20}$$
$$\mathcal{T}_k = \mathcal{T}_k(\dot{\varepsilon}_k) \tag{21}$$
$$\mathcal{R}_k = \mathcal{R}_k(\varepsilon_{k-1}, \varepsilon_k) \tag{22}$$
$$\tau_k = \tau_k(\dot{\varepsilon}_k, \dot{d}_k) \tag{23}$$
$$\tau_{k+1} = \tau_{k+1}(\dot{\varepsilon}_k, \varepsilon_k, \dot{d}_k, d_k) \tag{24}$$

with $\dot{\varepsilon}_k = \varepsilon_0, \varepsilon_1, \ldots, \varepsilon_{k-1}$ and $\dot{d}_k = d_0, d_1, \ldots, d_{k-1}$.

As the recursive formulation of LS provides at each step k the properties of the already reconstructed layers $(\dot{\varepsilon}_k, \dot{d}_k)$, the set of descriptors (20)–(24) becomes a system of two equations [(22) and (24)] with two unknowns (ε_k and d_k), which is consistent.

For lossy media, instead, permittivity is a complex value whose imaginary part takes into account the loss characteristics of the material [28] so that the five descriptors would depend also on conductivity

$$\mathcal{P}_k = \mathcal{P}_k(\dot{d}_k) \tag{25}$$
$$\mathcal{T}_k = \mathcal{T}_k(\dot{\varepsilon}_k, \dot{\sigma}_k) \tag{26}$$
$$\mathcal{R}_k = \mathcal{R}_k(\varepsilon_{k-1}, \varepsilon_k, \sigma_{k-1}, \sigma_k) \tag{27}$$
$$\tau_k = \tau_k(\dot{\varepsilon}_k, \varepsilon_k, \dot{\sigma}_k, \sigma_k, \dot{d}_k) \tag{28}$$
$$\tau_{k+1} = \tau_{k+1}(\dot{\varepsilon}_k, \varepsilon_k, \varepsilon_{k+1}, \dot{\sigma}_k, \sigma_k, \sigma_{k+1}, \dot{d}_k, d_k). \tag{29}$$

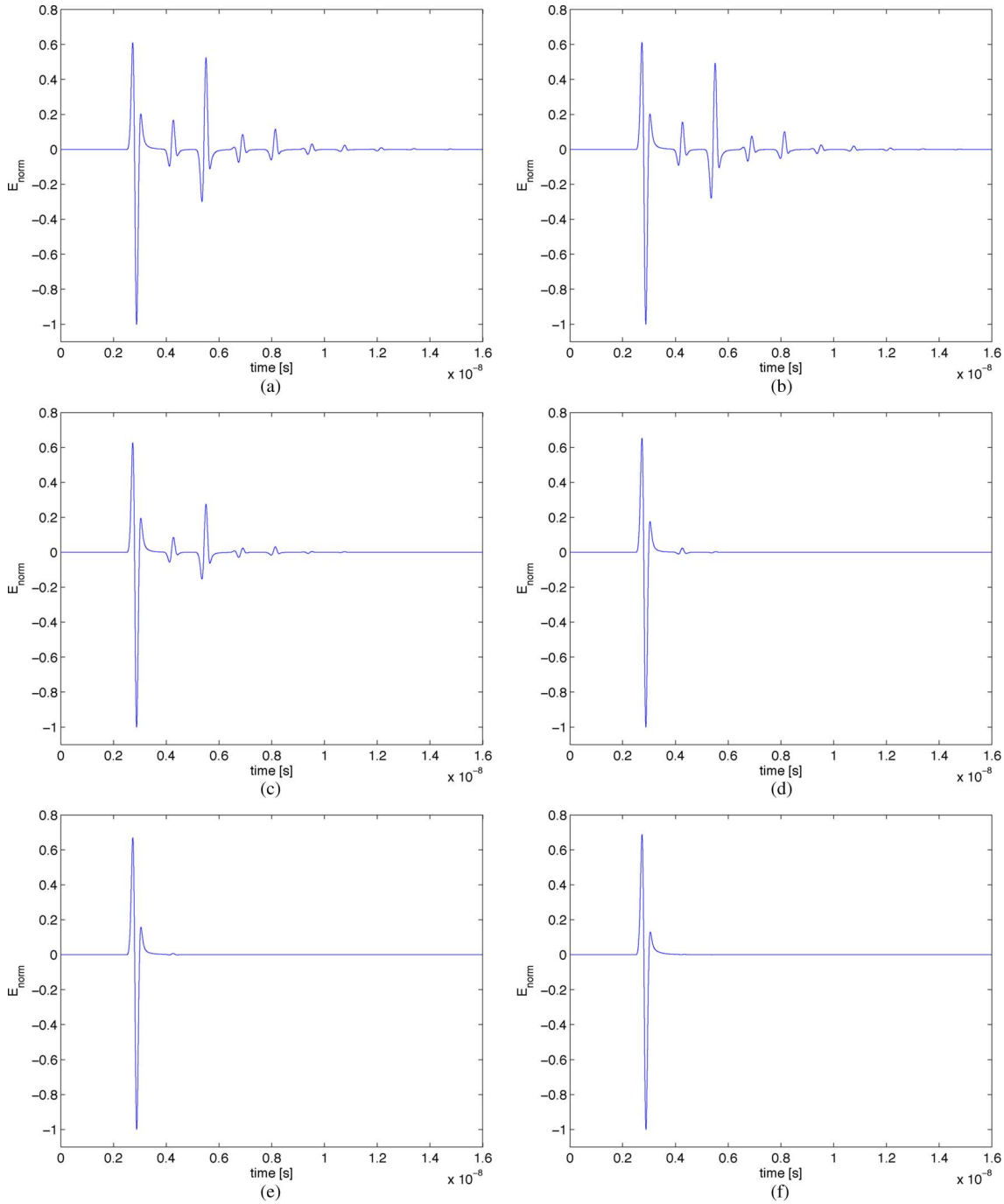

Fig. 13. Signals backscattered by lossy media characterized by different conductivity values (and fixed permittivity). (a) 0.00 S/m. (b) 0.01 S/m. (c) 0.10 S/m. (d) 0.30 S/m. (e) 0.50 S/m. (f) 1.00 S/m.

The set of descriptors (25)–(29) would therefore become a system of three equations [(27)–(29)] with five unknowns (ε_k, ε_{k+1}, σ_k, σ_{k+1}, and d_k), which is inconsistent.

Nevertheless, even though losses are not theoretically supported, in most applications, from geophysical surveys to infrastructure monitoring, test scenarios are characterized by low-loss materials [29], [30]; thus, we will show that the method, in such cases, could be suitably applied without limitations.

For this test, a new data set has been therefore simulated where each layer is modeled with an electric conductivity $\sigma_L =$ 0.01, 0.10, 0.30, 0.50, and 1.00 S/m.

In Fig. 13, we can see from a qualitative point of view how the received signals can significantly vary depending on the values of σ_L. In terms of reconstruction errors, reported in Table VII, there is no appreciable worsening of the performances when conductivity remains below 0.01 S/m, with mean relative errors comparable to those obtained for lossless media. When conductivity values are around 0.1 S/m, the accuracy starts reducing, with mean errors that jump to 6% and 25% for ε_1 and ε_2, respectively. The estimation of these permittivities is then significantly altered when σ_L rises to 0.3 S/m. As regards thicknesses d_1 and d_2, the error trend has a different behavior, with slopes that smoothly increase to error values remaining

TABLE VII
PERFORMANCE ASSESSMENT: CONDUCTIVITY

$\sigma_{1,2}$ [S/m]	ε_1	$\mathbf{d_1}$	ε_2	$\mathbf{d_2}$
0.01	1.63%	0.53%	5.40%	1.73%
0.10	6.89%	2.46%	25.25%	7.65%
0.30	23.96%	3.40%	46.50%	13.09%
0.50	37.65%	6.94%	73.86%	-
1.00	83.42%	-	-	-

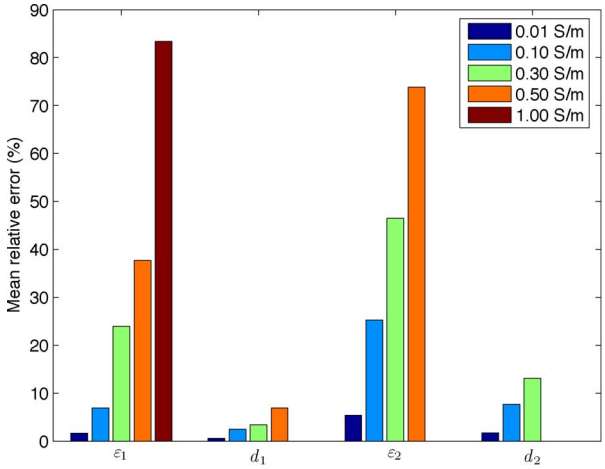

Fig. 14. Mean reconstruction errors versus conductivity.

below the acceptable threshold of 15% (see Fig. 14) also for the limit case $\sigma_L = 0.3$ S/m.

For greater values of conductivity ($\geq$ 0.5 S/m), in fact, some of the echoes of interest cannot be even detected, and no information can be provided about the thickness of the second layer. When $\sigma_L = 1$ S/m, the only echo that can be sensed by the receiver is the first bounce, which means that we would be able to determine only the permittivity of the first layer, whose reconstruction can be carried out with an error of 80%.

To conclude the analysis, it should be anyway pointed out that there is actually a very specific case where the current formulation can be theoretically employed to reconstruct also conductivity, i.e., a lossy slab comprised between two lossless media.

For the sake of simplicity, let us consider a slab characterized by ε_1, d_1, and σ_1 and immersed in air ($\varepsilon_0 = \varepsilon_2 = 1$ and $\sigma_0 = \sigma_2 = 0$). According to the previous discussion, we then have to use the following descriptors:

$$\mathcal{P}_1 = \mathcal{P}_1(d_0) \tag{30}$$
$$\mathcal{T}_1 = 1 \tag{31}$$
$$\mathcal{R}_1 = \mathcal{R}_1(\varepsilon_0, \varepsilon_1, \sigma_0, \sigma_1) \tag{32}$$
$$\tau_1 = \tau_1(\varepsilon_0, \varepsilon_1, \sigma_0, \sigma_1, d_0) \tag{33}$$
$$\tau_2 = \tau_2(\varepsilon_0, \varepsilon_1, \varepsilon_2, \sigma_0, \sigma_1, \sigma_2, d_0, d_1). \tag{34}$$

As ε_0, ε_2, σ_0, σ_2, and d_0 are *a priori* known, the set of descriptors (30)–(34) can be reduced to a system of three equations [(32)–(34)] in three unknowns $(\varepsilon_1, \sigma_1, d_1)$, which is now consistent. This kind of scenario can, for example, model a typical through-the-wall application, where the inversion algorithm could be employed to estimate the properties of a lossy wall.

TABLE VIII
ECHO CLASSIFICATION THROUGH MRR ROUTINE

Coefficients α_i	Propagation path	Class
100000	010	D
110000	01210	D
120000	0121210	M
111000	0123210	D
130000	012121210	M
121000	012123210	M
	012321210	M
112000	012323210	M
111100	012343210	D
140000	01212121210	M
131000	01212123210	M
	01212321210	M
	01232121210	M
122000	01212323210	M
	01232123210	M
	01232321210	M
111110	01234543210	D
113000	01232323210	M
121100	01212343210	M
	01234321210	M
150000	01212121210	M
111111	0123456543210	D

G. Feasibility of the Iterative Process

Section IV-A has shown that the reconstruction errors on the second layer are higher than those obtained for the first one. This is an intrinsic drawback of the LS approach due to its recursive formulation. In fact, as the number of layers increases, more iterations are required, so performances experience a general worsening due to the error spreading from one layer to the subsequent one, resulting in a divergent reconstruction [31].

In this last part of the section, we will therefore want to evaluate if the proposed method is feasible to handle complex scenarios and provide sufficient accuracies also for the deepest slabs.

The simulated test case for this analysis is a five-layer medium, with the following characteristics:

$$\begin{aligned}
L_1: &\quad \varepsilon_1 = 10, \quad \mu_1 = 1, \quad \sigma_1 = 0 \text{ S/m}, \quad d_1 = 0.08 \text{ m} \\
L_2: &\quad \varepsilon_2 = 7, \quad \mu_2 = 1, \quad \sigma_2 = 0 \text{ S/m}, \quad d_2 = 0.12 \text{ m} \\
L_3: &\quad \varepsilon_3 = 4, \quad \mu_3 = 1, \quad \sigma_3 = 0 \text{ S/m}, \quad d_3 = 0.20 \text{ m} \\
L_4: &\quad \varepsilon_4 = 13, \quad \mu_4 = 1, \quad \sigma_4 = 0 \text{ S/m}, \quad d_4 = 0.05 \text{ m} \\
L_5: &\quad \varepsilon_5 = 19, \quad \mu_5 = 1, \quad \sigma_5 = 0 \text{ S/m}, \quad d_5 = 0.03 \text{ m}.
\end{aligned}$$

The overall received signals have been scanned to detect and classify the echoes through the MRR procedure, which groups the signals into two categories, direct reflections (D), to be inverted, and multiple reflections (M), to be suppressed. The complete classification output of the MRR routine is reported in Table VIII, where the first column contains the coefficients α_i enforcing (13), the second column lists the propagation paths of the echoes (each number corresponds to the interface reached by the wave, so "0" indicates interface I_0, "1" indicates interface I_1, etc.), and the third column specifies the class.

The reconstruction process can be qualitatively evaluated in Fig. 15, showing the actual and reconstructed profile of the multilayered medium. It can be noticed that, for the first three layers, there is a very good matching between the two curves, which then feature a progressive permittivity mismatch for layers L_4 and L_5. As far as the thickness is concerned, instead, no sensible worsening of the performances can be observed.

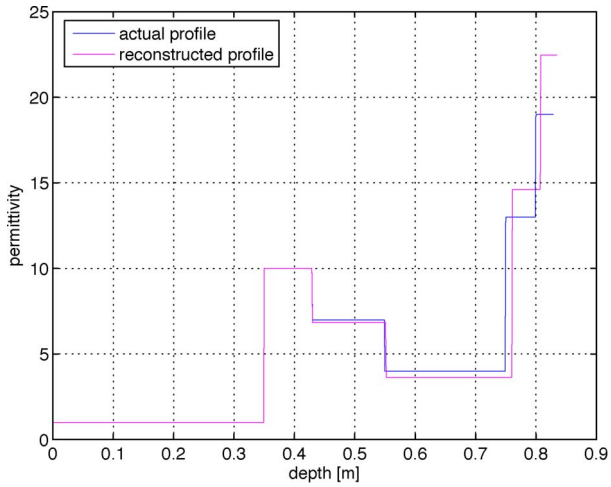

Fig. 15. Actual and reconstructed profile of the five-layer medium (blue and magenta curves, respectively).

TABLE IX
PERFORMANCE ASSESSMENT: FIVE LAYERS

	Permittivity		Thickness	
	δ_ε	$\delta_{\varepsilon_\%}$	δ_d [mm]	$\delta_{d_\%}$
Layer 1	0.06	0.60%	0.2	0.31%
Layer 2	0.19	2.74%	1.9	1.60%
Layer 3	0.37	9.45%	2.1	1.04%
Layer 4	1.15	8.88%	2.0	4.05%
Layer 5	2.18	11.50%	2.2	7.43%

Getting into numerical details (see Table IX), we can find that the reconstruction errors for layers L_1, L_2, and L_3 are totally in line with those discussed in Sections IV-A and D, with permittivity relative error increasing from 0.05% to 9% and absolute error not exceeding 0.5. Accuracy starts diminishing from layer L_4, whose permittivity is reconstructed with an error of 1.15, and as expected, the worst performance is obtained for ε_5, reconstructed with an error of 2.18. The general error trend confirms that, at each step, the reconstruction accuracy is biased by the errors accumulated within the previous iterations, limiting the total number of layers that can be processed. Nevertheless, the overall performances can be still considered acceptable even for the deepest layers.

We can notice a completely different trend within the reconstructed values of thickness, which is provided with very high accuracy for all the layers. The relative error slightly increases from 0.02% to 7%, but the absolute error is always below the noticeable threshold of 0.3 cm, and its behavior is not monotone (e.g., $d_1 < d_2$, but $d_2 > d_3$). As previously stressed, this is due to the fact that the computation of echoes' time delays is reinitialized at each iteration, so it does not suffer an error propagation within layers.

The feasibility of the iterative process has been also tested in the presence of noisy data, obtained as in Section IV-E, by adding white Gaussian noise according to different SNR levels (5, 10, 20, 30, and 40 dB). Results are reported in Table X. Again, permittivity reconstruction strongly depends on signals' amplitudes, so an increase of the errors due to higher levels of noise can be noticed. In addition, the accumulation of the errors from layer to layer hinders the reconstruction of deeper layers,

TABLE X
PERFORMANCE ASSESSMENT: FIVE LAYERS WITH AWGN

SNR		Permittivity		Thickness	
		δ_ε	$\delta_{\varepsilon_\%}$	δ_d [mm]	$\delta_{d_\%}$
5 dB	Layer 1	0.49	4.90%	3.8	4.72%
	Layer 2	0.61	8.71%	1.2	1.05%
	Layer 3	0.77	19.25%	5.4	2.69%
	Layer 4	2.65	20.40%	3.9	7.82%
	Layer 5	5.23	27.55%	2.7	9.03%
10 dB	Layer 1	0.24	2.48%	1.0	1.25%
	Layer 2	0.27	3.97%	2.7	2.25%
	Layer 3	0.44	11.12%	3.1	15.61%
	Layer 4	1.83	14.10%	2.1	4.22%
	Layer 5	4.04	21.29%	1.3	4.40%
20 dB	Layer 1	0.12	1.20%	0.5	0.63%
	Layer 2	0.23	3.34%	2.3	1.92%
	Layer 3	0.39	9.82%	2.5	1.25%
	Layer 4	1.54	11.86%	1.7	3.50%
	Layer 5	3.44	18.13%	1.5	5.73%
30 dB	Layer 1	0.09	0.93%	0.4	0.56%
	Layer 2	0.21	3.05%	2.1	1.78%
	Layer 3	0.38	9.55%	2.2	1.11%
	Layer 4	1.29	9.94%	1.8	3.64%
	Layer 5	2.79	14.68%	1.9	6.36%
40 dB	Layer 1	0.06	0.67%	0.3	0.38%
	Layer 2	0.19	2.78%	1.4	1.18%
	Layer 3	0.35	8.75%	2.1	1.06%
	Layer 4	1.17	9.02%	1.8	3.68%
	Layer 5	2.23	11.71%	2.2	7.33%

and consequently, the worst performances are obtained for L_5 at 5-dB SNR. Nevertheless, considering the strong distortion of the signals, a relative error of 27.55% (almost 2.5 times the noise-free case) is quite satisfactory.

As regards thickness reconstruction, instead, we have already stressed that it is less sensitive to noise, so results do not experience a noticeable worsening. Even in the 5-dB SNR case, which still remains the most awkward condition, the maximum absolute error is only of 5.4 mm.

V. CONCLUSION

In this paper, an LS approach for the EM reconstruction of stratified media has been presented.

In particular, an equalization step has been introduced, which takes into account the effects of wave propagation, showing that the choice of a proper propagation model can provide higher accuracies. The processing chain has been also supplied with a subroutine for the identification and classification of multiple reflections that has been exploited to filter the received signal and therefore enhance the reconstruction process. Moreover, an energy-based method specifically conceived to detect echoes' amplitudes and TODs has proven its effectiveness and revealed good capabilities in resolving overlapping signals.

On the other hand, the principal drawback suffered by LS methods regards their recursive formulation, which causes the accumulation of reconstruction errors from one layer to the other. A five-layer medium has been therefore studied to test the feasibility of the iterative process, showing that reconstruction accuracy progressively reduces but remains acceptable until the last step. Furthermore, the proposed approach is based on the theoretical assumption of lossless nondispersive media; we have anyway shown that low-loss dielectrics can be still processed with no significant worsening of the performances.

Results remain acceptable also in the presence of low values of SNR.

To improve the overall results, further developments could involve a new formulation able to reduce the effects of noise and to theoretically take into account losses, for instance, by means of a multiview/multisource approach.

REFERENCES

[1] K. Golden, D. Borup, M. Cheney, E. Cherkaeva, M. Dawson, K.-H. Ding, A. Fung, D. Isaacson, S. Johnson, A. Jordan, J. A. Kon, R. Kwok, S. Nghiem, R. Onstott, J. Sylvester, D. Winebrenner, and I. Zabel, "Inverse electromagnetic scattering models for sea ice," *IEEE Trans. Geosci. Remote Sens.*, vol. 36, no. 5, pp. 1675–1704, Sep. 1998.

[2] F. Soldovieri, R. Solimene, A. Brancaccio, and R. Pierri, "Localization of the interfaces of a slab hidden behind a wall," *IEEE Trans. Geosci. Remote Sens.*, vol. 45, no. 8, pp. 2471–2482, Aug. 2007.

[3] R. Roberts, A. Schutz, I. Al-Qadi, and E. Tutumluer, "Characterizing railroad ballast using GPR: Recent experiences in the United States," in *Proc. 4th Int. Workshop Adv. Ground Penetrating Radar*, Jun. 2007, pp. 295–299.

[4] S. Lambot, E. Slob, I. van den Bosch, B. Stockbroeckx, and M. Vanclooster, "Modeling of ground-penetrating radar for accurate characterization of subsurface electric properties," *IEEE Trans. Geosci. Remote Sens.*, vol. 42, no. 11, pp. 2555–2568, Nov. 2004.

[5] B. Levy, "Layer by layer reconstruction methods for the earth resistivity from direct current measurements," *IEEE Trans. Geosci. Remote Sens.*, vol. GE-23, no. 6, pp. 841–850, Nov. 1985.

[6] J. Sylvester, D. Winebrenner, and F. Gylys-Colwell, "Layer stripping for the Helmholtz equation," *SIAM J. Appl. Math.*, vol. 56, no. 3, pp. 736–754, Jun. 1996.

[7] A. Loizos and C. Plati, "Accuracy of ground penetrating radar horn-antenna technique for sensing pavement subsurface," *IEEE Sensors J.*, vol. 7, no. 5, pp. 842–850, May 2007.

[8] M. P. H. Andresen, H. E. Krogstad, and J. Skaar, "Inverse scattering of two-dimensional photonic structures by layer stripping," *J. Opt. Soc. Amer. B*, vol. 28, no. 4, pp. 689–696, Apr. 2011.

[9] S. Rao, *Time Domain Electromagnetics*. Amsterdam, The Netherlands: Elsevier, 1999, ser. Academic Press Series in Engineering.

[10] A. E. Yagle and P. Raadhakrishnan, "Numerical performance of layer stripping algorithms for two-dimensional inverse scattering problems," *Inverse Problems*, vol. 8, no. 4, p. 645, Aug. 1992.

[11] A. E. Yagle and B. C. Levy, "The Schur algorithm and its applications," *Acta Applicandae Mathematicae*, vol. 3, no. 3, pp. 255–284, May 1985.

[12] U. Spagnolini and V. Rampa, "Multitarget detection/tracking for monostatic ground penetrating radar: Application to pavement profiling," *IEEE Trans. Geosci. Remote Sens.*, vol. 37, no. 1, pp. 383–394, Jan. 1999.

[13] U. Spagnolini, "Permittivity measurements of multilayered media with monostatic pulse radar," *IEEE Trans. Geosci. Remote Sens.*, vol. 35, no. 2, pp. 454–463, Mar. 1997.

[14] T. Saarenketo and T. Scullion, "Road evaluation with ground penetrating radar," *J. Appl. Geophys.*, vol. 43, no. 2–4, pp. 119–138, Mar. 2000.

[15] I. AL-Qadi and S. Lahouar, "Measuring layer thicknesses with GPR—Theory to practice," *Construction Building Mater.*, vol. 19, no. 10, pp. 763–772, Dec. 2005.

[16] J. S. Lee, C. Nguyen, and T. Scullion, "A novel, compact, low-cost, impulse ground-penetrating radar for nondestructive evaluation of pavements," *IEEE Trans. Instrum. Meas.*, vol. 53, no. 6, pp. 1502–1509, Dec. 2004.

[17] J. Frolik, "Reconstruction of multilayered lossy dielectrics from one-sided plane wave impulse reflection responses: The bistatic case," *IEEE Trans. Geosci. Remote Sens.*, vol. 39, no. 9, pp. 2051–2059, Sep. 2001.

[18] S. Lahouar and I. L. Al-Qadi, "Automatic detection of multiple pavement layers from GPR data," *NDT&E International*, vol. 41, no. 2, pp. 69–81, Mar. 2008.

[19] C. Huang and Y. Su, "A new GPR calibration method for high accuracy thickness and permittivity measurement of multi-layered pavement," in *Proc. 10th Int. Conf. GPR*, Jun. 2004, pp. 627–630.

[20] P. K. Verma, A. N. Gaikwad, D. Singh, and M. J. Nigam, "Analysis of clutter reduction techniques for through wall imaging in UWB range," *Progress Electromagn. Res. B*, vol. 17, pp. 29–48, 2009.

[21] C. Le Bastard, V. Baltazart, Y. Wang, and J. Saillard, "Thin-pavement thickness estimation using GPR with high-resolution and superresolution methods," *IEEE Trans. Geosci. Remote Sens.*, vol. 45, no. 8, pp. 2511–2519, Aug. 2007.

[22] C. A. Balanis, *Modern Antenna Handbook*. New York, NY, USA: Wiley-Interscience, 2008.

[23] S. Caorsi and M. Stasolla, "Towards the detection of multiple reflections in time-domain EM inverse scattering of multi-layered media," *Progress Electromagn. Res. B*, vol. 38, pp. 351–365, 2012.

[24] A. Giannopoulos, "Modelling ground penetrating radar by GprMax," *Construction Building Mater.*, vol. 19, no. 10, pp. 755–762, Dec. 2005.

[25] K. Belli, C. Rappaport, H. Zhan, and S. Wadia-Fascetti, "Effectiveness of 2-D and 2.5-D FDTD ground-penetrating radar modeling for bridge-deck deterioration evaluated by 3-D FDTD," *IEEE Trans. Geosci. Remote Sens.*, vol. 47, no. 11, pp. 3656–3663, Nov. 2009.

[26] J. S. Juntunen and T. D. Tsiboukis, "Reduction of numerical dispersion in FDTD method through artificial anisotropy," *IEEE Trans. Microw. Theory Tech.*, vol. 48, no. 4, pp. 582–588, Apr. 2000.

[27] J. B. Schneider and C. L. Wagner, "FDTD dispersion revisited: Faster-than-light propagation," *IEEE Microw. Guided Wave Lett.*, vol. 9, no. 2, pp. 54–56, Feb. 1999.

[28] D. Pozar, *Microwave Engineering*. Hoboken, NJ, USA: Wiley, 1997.

[29] J. Hipp, "Soil electromagnetic parameters as functions of frequency, soil density, and soil moisture," *Proc. IEEE*, vol. 62, no. 1, pp. 98–103, Jan. 1974.

[30] S. Vitebskiy, L. Carin, M. Ressler, and F. Le, "Ultra-wideband, short-pulse ground-penetrating radar: Simulation and measurement," *IEEE Trans. Geosci. Remote Sens.*, vol. 35, no. 3, pp. 762–772, May 1997.

[31] J. Frolik, "On the feasibility of impulse reflection response data from one-dimensional multilayered lossy media," *IEEE Trans. Antennas Propag.*, vol. 51, no. 2, pp. 184–194, Feb. 2003.

Salvatore Caorsi (M'99) received the Laurea degree in electronics engineering from the University of Genoa, Genoa, Italy.

Since 1976, he has been a Professor of antennas and also of remote sensing and electromagnetic diagnostics with the University of Genoa. Since 1994, he has been a Full Professor at the University of Pavia, Pavia, Italy, where he teaches electromagnetic compatibility, electromagnetic techniques for remote sensing and diagnostics, electromagnetic fields, and environment impact. His primary activities focus on the evaluation of electromagnetic fields in the complex domain, nonlinear scattering, electromagnetic compatibility, bioelectromagnetic interaction, inverse scattering, and, in particular, electromagnetic techniques for remote sensing and diagnostics. He has been the chairman for many research units in national and international research projects and the organizer of national and international congresses and symposia as well as of scientific sessions and workshops. He has been the President and founding member of the national Inter-University Research Centre for the Interactions between Electromagnetic fields and Biological Systems (ICEmB), for which he is currently the Director.

Prof. Caorsi is a reviewer for some international scientific journals such as the IEEE TRANSACTIONS ON MICROWAVE THEORY AND TECHNIQUES and IEEE TRANSACTIONS ON ANTENNAS AND PROPAGATION. He is a member of the European Bioelectromagnetic Association (EBEA).

Mattia Stasolla (S'06–M'10) received the B.Sc. degree in electronics and telecommunications engineering, the M.Sc. degree in electronics engineering, and the Ph.D. degree in electronics and computer science from the University of Pavia, Pavia, Italy, in 2003, 2005, and 2008, respectively. In 2006, he also received the diploma for sciences and technologies class from the Institute for Advanced Studies (IUSS) of Pavia.

From 2009 to 2013, he was a Research Fellow at the University of Pavia. In 2013, he joined the European Commission Joint Research Center, Institute for the Protection and Security of the Citizen. His fields of interest include RADAR and optical data processing, direct and inverse scattering problems, mathematical morphology, fuzzy rule-based classifiers, and neural networks. His main research activity focuses on the exploitation of remote sensing technology for protection and security.

Dr. Stasolla frequently acts as a referee for the IEEE TRANSACTIONS ON GEOSCIENCE AND REMOTE SENSING, the IEEE JOURNAL OF SELECTED TOPICS IN APPLIED EARTH OBSERVATIONS, and the IEEE GEOSCIENCE AND REMOTE SENSING LETTERS.